Neurobiology of Stress 15 (2021) 100363

Contents lists available at ScienceDirect

Neurobiology of Stress

journal homepage: www.elsevier.com/locate/ynstr

Glucagon-like peptide 1 receptor-mediated stimulation of a GABAergic projection from the bed nucleus of the stria terminalis to the hypothalamic paraventricular nucleus

Nadya Povysheva [a], Huiyuan Zheng [b], Linda Rinaman [b,*]

[a] Department of Neuroscience, University of Pittsburgh, Pittsburgh, PA, 15260, USA
[b] Department of Psychology, Program in Neuroscience, Florida State University, Tallahassee, FL, 32306, USA

ARTICLE INFO

Keywords:
Ex vivo slice
Whole-cell patch recording
GABA
Glutamate
Vgat
Vglut2
GLP1
GLP1R
HPA axis
In situ hybridization
Rat

ABSTRACT

We previously reported that GABAergic neurons within the ventral anterior lateral bed nucleus of the stria terminalis (alBST) express glucagon-like peptide 1 receptor (GLP1R) in rats, and that virally-mediated "knock-down" of *GLP1R* expression in the alBST prolongs the hypothalamic-pituitary-adrenal axis response to acute stress. Given other evidence that a GABAergic projection pathway from ventral alBST serves to limit stress-induced activation of the HPA axis, we hypothesized that GLP1 signaling promotes activation of GABAergic ventral alBST neurons that project directly to the paraventricular nucleus of the hypothalamus (PVN). After PVN microinjection of fluorescent retrograde tracer followed by preparation of *ex vivo* rat brain slices, whole-cell patch clamp recordings were made in identified PVN-projecting neurons within the ventral alBST. Bath application of Exendin-4 (a specific GLP1R agonist) indirectly depolarized PVN-projecting neurons in the ventral alBST and adjacent hypothalamic parastrial nucleus (PS) through a network-dependent increase in excitatory synaptic inputs, coupled with a network-independent reduction in inhibitory inputs. Additional retrograde tracing experiments combined with *in situ* hybridization confirmed that PVN-projecting neurons within the ventral alBST/PS are GABAergic, and do not express *GLP1R* mRNA. Conversely, *GLP1R* mRNA is expressed by a subset of neurons that project into the ventral alBST and were likely contained within coronal *ex vivo* slices, including GABAergic neurons within the oval subnucleus of the dorsal alBST and glutamatergic neurons within the substantia innominata. Our novel findings reveal potential GLP1R-mediated mechanisms through which the alBST exerts inhibitory control over the endocrine HPA axis.

1. Introduction

In rats and mice, physiological and behavioral stress responses are elicited and/or enhanced by increasing glucagon-like peptide-1 (GLP1) signaling within the brain, and are attenuated by reducing central GLP1 signaling (vanDijk and Thiele, 1999) (Kinzig et al., 2003) (Maniscalco et al., 2013) (Maniscalco et al., 2015) (Holt and Trapp, 2016) (Maniscalco and Rinaman, 2017) (Holt et al., 2019). GLP1 receptors (GLP1R) are expressed in multiple stress-related brain regions that receive direct axonal input from GLP1-positive neurons in the caudal nucleus of the solitary tract (NST) and adjacent intermediate reticular formation (Cork et al., 2015) (Heppner et al., 2015). These target regions include the anterior lateral bed nucleus of the stria terminalis (alBST), a limbic forebrain structure implicated in the central control of autonomic, neuroendocrine, and behavioral outflow (Dong and Swanson, 2006a) (Dong and Swanson, 2006b) (Crestani et al., 2013) (Johnson et al., 2016) (Johnson et al., 2019).

In recent years, rodent models have been used to examine how hindbrain GLP1 neural inputs to the alBST modulate the ability of acute stress to suppress food intake, promote anxiety-like behavior, and increase plasma levels of stress hormone [i.e., corticosterone (cort)] (Williams et al., 2018) (Zheng et al., 2019). We reported that virally-mediated suppression of *GLP1R* mRNA translation in the alBST has anxiolytic behavioral effects in rats, but paradoxically prolongs the plasma cort response to acute stress (Zheng et al., 2019). We interpreted the latter result as evidence that GLP1 signaling within the alBST normally engages an inhibitory "brake" on stress-induced activation of the hypothalamic-pituitary-adrenal (HPA) axis. This interpretation was

* Corresponding author. Program in Neuroscience, Florida State University, 1107 W Call Street, Tallahassee, FL, 32306, USA.
E-mail address: LRinaman@fsu.edu (L. Rinaman).

https://doi.org/10.1016/j.ynstr.2021.100363
Received 4 March 2021; Received in revised form 25 June 2021; Accepted 26 June 2021
Available online 2 July 2021

bolstered by our finding that *GLP1R*-expressing neurons in the ventral alBST are GABAergic (Zheng et al., 2019), consistent with evidence that a GABAergic projection pathway from the ventral alBST to the paraventricular nucleus of the hypothalamus (PVN) serves to restrain stress-induced activation of the HPA axis (Radley et al., 2009) (Johnson et al., 2016). Further, *GLP1R*-expressing neurons in the dorsal and/or ventral alBST send axonal projections to the PVN and other stress-related brain regions in mice (Williams et al., 2018). In the same mouse study, whole-cell patch clamp recordings conducted in *ex vivo* slices revealed that bath-applied GLP1 evokes direct depolarizing or hyperpolarizing postsynaptic responses in *GLP1R*-expressing neurons in both dorsal and ventral portions of the alBST (Williams et al., 2018), evidence for complex *GLP1R*-mediated neural responses within this limbic forebrain structure. However, as neither the subnuclear distribution nor the projection targets of identified GLP1-responsive alBST neurons was examined, it remains unclear whether and how GLP1 affects the electrophysiological properties of PVN-projecting neurons within the ventral alBST.

Based on the evidence summarized above, we recently speculated that *GLP1R* is expressed by PVN-projecting GABAergic neurons within the ventral alBST, and hypothesized that GLP1 directly depolarizes/activates these inhibitory projection neurons (Zheng et al., 2019). The present study was designed to test this hypothesis directly in rats. In the first experiment, a fluorescent retrobead labeling strategy was combined with whole-cell patch recordings in *ex vivo* slices to identify PVN-projecting neurons within the ventral alBST, and to examine responses of these neurons to bath application of a specific GLP1R agonist. In the second experiment, a more sensitive retrograde tracer was combined with RNAscope fluorescent *in situ* hybridization to document the neurotransmitter phenotype of PVN-projecting neurons located in distinct subregions of the ventral alBST and adjacent parastrial nucleus (PS) of the hypothalamic preoptic region, and to determine whether these PVN-projecting neurons express mRNA for *GLP1R*. In a final follow-up experiment, retrograde labeling was combined with *in situ* hybridization to examine *GLP1R* mRNA expression in neurons that provide input to the ventral alBST, and whose axonal projections may have been intact within coronal *ex vivo* slices.

2. Methods

All animal procedures were conducted in accordance with the National Institutes of Health Guide for the Care and Use of Laboratory Animals (2011), and were approved by the Institutional Animal Care and Use Committee at the University of Pittsburgh and/or Florida State University.

2.1. Electrophysiological analysis of PVN-projecting neurons in the ventral alBST

2.1.1. Retrograde labeling

PVN-projecting neurons were retrogradely labeled for subsequent collection of electrophysiological data in *ex vivo* slices. Young adult male Sprague-Dawley rats (Harlan; 180–190 g BW) were anesthetized by isoflurane inhalation (1–3% in oxygen; Halocarbon Laboratories) and fixed into a stereotaxic device in the flat skull position. Undiluted Red IX Retrobeads (LumaFluor, Inc. USA) were delivered by pressure (200 nl/injection, 100 nl/min) into the PVN bilaterally (coordinates from bregma: −1.90 mm posterior, 0.30 mm lateral, −7.90 mm ventral) using a glass micropipette (~20 μm outer tip diameter) connected to a 10 μl Hamilton syringe controlled by a digital stereotaxic microinjector (catalog #QSI 53311, Stoelting). After each injection, the micropipette was left in place for 5 min to minimize tracer backflow. After the injector was removed, the skin over the skull was closed with 4-0 nylon sutures. Rats were injected subcutaneously with ketofen (2 mg/kg BW) and buprenorphine (0.03 mg/kg BW) and were returned to their home cages after full recovery from anesthesia.

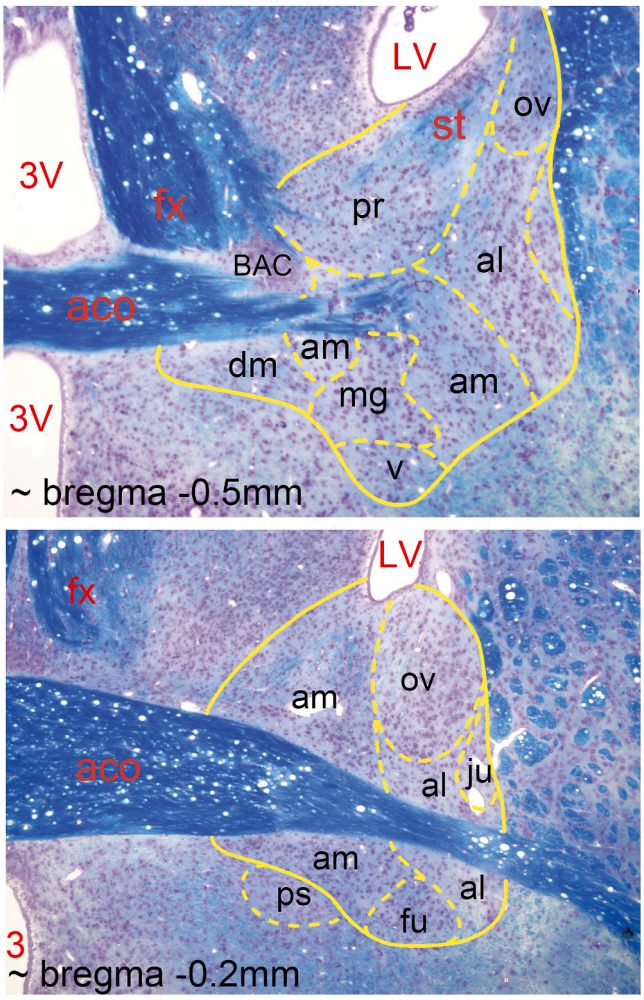

Fig. 1. Subnuclear organization of the rat alBST.
Klüver-Barrera-stained coronal tissue sections through two representative rostrocaudal levels of the alBST. Myelinated fibers are blue, neuron cell bodies are pink/purple. Images are adapted from our previous publication (Bienkowski et al., 2013), with BST subnuclei outlined in yellow and labeled according to the most recent version of Swanson's rat brain atlas (Swanson, 2018). 3V, third ventricle; aco, anterior commissure; al, anterolateral subnucleus; am, anteromedial subnucleus; BAC, bed nucleus anterior commissure; dm, dorsomedial subnucleus, fu, fusiform subnucleus; fx, fornix; ju, juxtacapsular subnucleus; LV, lateral ventricle; mg, magnocellular subnucleus; ov, oval subnucleus; pr, principal subnucleus; ps, parastrial subnucleus of the hypothalamus; st, stria terminalis; v, ventral subnucleus. The approximate (~) rostro-caudal level of each section (relevant to bregma) is indicated; the more caudal section is at the top, and the more rostral section at the bottom. (For interpretation of the references to colour in this figure legend, the reader is referred to the Web version of this article.)

2.1.2. Whole-cell patch clamp recordings

One week after stereotaxic Retrobead tracer injection into the PVN, rats were deeply anesthetized with isoflurane (5% in oxygen via inhalation) and then decapitated. The brain was quickly removed and immersed in ice-cold pre-oxygenated artificial cerebrospinal fluid (ACSF). A tissue block containing the anterior BST was excised, and coronal slices (350–400 μm thick) were cut with a vibratome (Leica VT1000S, Leica, Germany). Visual landmarks including the anterior commissure, lateral ventricles, and optic chiasm were used to select slices through the appropriate rostrocaudal level of the anterior BST [i.e., approximately 0.2–0.5 mm caudal to bregma, based on the most recent version of Swanson's rat brain atlas (Swanson, 2018); see Fig. 1]. Slices were incubated at 37°C for 0.5–1 h, then kept at room temperature

before being transferred to a recording chamber perfused with oxygenated ACSF (95% O_2/5% CO_2; pH 7.25–7.3) at 31–32°C. ACSF solution composition (in mM) was 126 NaCl, 2.5 KCl, 1.25 NaH_2PO_4, 1 $MgSO_4$, 2 $CaCl_2$, 24 $NaHCO_3$, and 10–20 glucose.

A Zeiss Axioskop microscope (Carl Zeiss, Inc., Thornwood, NY) equipped with a 40× water immersion objective and a digital video camera (CoolSnap, Photometrics, Tucson, Az) was used to visualize retrogradely-labeled neurons for whole-cell recordings. Within each slice, the ventral region of the alBST was identified by its medial-lateral position (i.e., vertically aligned with the lateral ventricle, medial to the internal capsule), by its close ventral proximity to the anterior commissure, and by the presence of red retrobead-labeled neurons. Patch electrodes were filled with an internal solution containing (in mM): 105 Cs-gluconate, 2 $MgCl_2$, 10 NaCl, 10 HEPES, 10 phosphocreatine, 4 ATP-Mg, 0.3 GTP, and 10 BAPTA; pH 7.25. In addition, Alexa 568 (0.075%; Molecular Probes, Eugene, OR) was added to the intracellular solution to fill each recorded neuron for later morphological identification, as previously described (Povysheva et al., 2006). Electrodes had 5–10 MΩ open-tip resistance. Voltage and current recordings were performed with a Multi-Clamp 700A amplifier (Axon Instruments, Union City, CA). Voltage recordings were performed in bridge-balance mode. Signals were filtered at 2 KHz, and acquired at a sampling rate of 10 kHz using a Digidata 1440 digitizer and Clampex 10.2 software (Molecular Devices Corporation, Sunnyvale, CA). Access resistance and capacitance were compensated on-line. Access resistance typically was 10–20 MΩ and remained relatively stable during experiments (≤30% increase) for cells included in data analysis. Membrane potential was corrected for the liquid junction potential of −13 mV.

The synthetic GLP1 analogue Exendin-4 (Ex-4; 200–600 nM; Bachem, Torrance, CA) was bath-applied to activate GLP1Rs, while the specific antagonist Exendin-9 (Ex-9; 900 nM; Bachem) was used to block GLP1Rs (Goke et al., 1993) (Thorens et al., 1993). Additional pharmacological agents were bath applied at the following concentrations: tetrodotoxin (TTX; 0.5 μM; Sigma) to block voltage-gated Na^+ channels; AP-5 (D-2-amino-5-phospho-pentanoic acid; 50 μM; Ascent Scientific LTD, Bristol, UK) to block NMDA (N-methyl-D-aspartate) receptors; NBQX (2,3-dihydroxy-6-nitro-7-sulfamoylbenzo(F)quinoxaline; 20 μM; Ascent Scientific) to block AMPA (α-amino-3--hydroxy-5-methyl-4-isoxazolepropionic acid) and kainate receptors; gabazine (10 μM; Ascent Scientific LTD, Bristol, UK) to block $GABA_A$ receptors.

Patch-clamp recordings in identified ventral alBST neurons were made in the presence or absence of Ex-4. Spontaneous firing frequency was estimated during 2 min intervals before and after bath application of Ex-4, with the latter interval beginning 1 min after application. Spontaneous inhibitory post-synaptic currents (sIPSCs) were recorded at a holding potential of +12 mV in the presence of NBQX and AP-5. Miniature inhibitory post-synaptic currents (mIPSCs) were recorded at a holding potential of +12 mV in the presence of TTX to inhibit action potential-mediated inhibitory postsynaptic currents. Spontaneous excitatory post-synaptic currents (sEPSCs) were recorded at a holding potential of −70 mV. Miniature excitatory post-synaptic currents (mEPSCs) were recorded at a holding potential of −70 mV in the presence of TTX to inhibit action potential-mediated excitatory postsynaptic currents. Spontaneous and miniature events were analyzed using the MiniAnalysis Program (Synaptosoft, Decatur, GA). Peak events were first detected automatically using an amplitude threshold of 1.5 times the average RMS noise, which approximated 3 pA for recordings at a holding potential of −70mV. More than 500 events per cell were included in each analysis.

To characterize neuronal membrane properties, hyper- and depolarizing current steps were applied for 500 ms in increments of 5–10 pA at 0.5 Hz. Input resistance was measured from the slope of a linear regression fit to the voltage-current relation in a voltage range hyperpolarized from resting potential. The membrane time constant was determined by single-exponential fitting to the average voltage responses activated by hyperpolarizing current steps of 5–15 pA. Action potential (AP) properties were quantified using the first action potential evoked through application of depolarizing current steps. AP threshold was measured at the level of voltage deflection exceeding 10 mV/1 ms. Peak AP amplitudes of the AP and afterhyperpolarization were measured relative to AP threshold. AP duration was measured at the base (AP threshold level). Action potential frequency was calculated in Hz as a ratio between number of action potentials and current step duration at 60 pA above the rheobase.

Neurons were filled with Alexa 568 during whole-cell recordings. A subset of these were maintained for at least 30 min to ensure extensive dendritic labeling. After recording, slices were fixed in ice-cold 4% paraformaldehyde for at least 72 h, then transferred into an anti-freeze solution (ethylene glycol and glycerol in 0.1 M phosphate buffer) and stored at −20°C. A few representative labeled neurons were reconstructed three-dimensionally using an Olympus Fluoview BX61 confocal microscope and Fluoview software (Olympus America Inc, Melville, NY).

2.1.3. Statistical analysis of electrophysiological data

Unless otherwise specified, one-way ANOVA and post-hoc two-tailed paired t-tests were used for between-group comparisons. Values are presented as mean ± SEM. Statistical tests were performed using Excel (Microsoft Corp., Redmond, WA). Effects were considered significant when $p < 0.05$.

2.4. Molecular phenotyping of projection-specific alBST neurons

2.4.1. Retrograde labeling

In a separate experiment, PVN-projecting neurons were retrogradely labeled and visualized using immunocytochemical detection of cholera toxin beta (CTB) neural tracer combined with dual *in situ* hybridization to analyze cellular expression of *GLP1R* plus *Vgat* mRNAs to identify GABAergic neurons, or *GLP1R* plus *Vglut2* mRNAs to identify glutamatergic neurons. For this, adult male Sprague-Dawley rats (n = 3; 225–250 g BW) were anesthetized by isoflurane inhalation (1–3% in oxygen; Halocarbon Laboratories) and placed into a stereotaxic device in the flat skull position. A pulled glass pipette (~20 μm outer tip diameter) was attached to the arm of the stereotaxic apparatus. A solution of 0.25% CTB (List Biological Labs, Campbell, CA, USA) in sodium phosphate buffer (pH 7.5) was backfilled through the pipette tip using negative pressure, then a wire connected to a current source (Stoelting) was inserted into the tracer solution. During descent of the glass pipette into the brain, a −0.5 μA retaining current was used to minimize molecular diffusion of tracer from the pipette tip. CTB was iontophoresed unilaterally into the PVN (from bregma: 1.90 mm posterior, 0.30 mm lateral, −7.90 mm ventral) using a 7 s on/off pulsed current of +5 μA for 10 min. Five minutes after the end of iontophoresis, a −0.5 μA retaining current was held as the pipette was withdrawn, and the skin over the skull was closed with 4-0 nylon sutures. Rats were injected subcutaneously with ketofen (2 mg/kg BW) and buprenorphine (0.03 mg/kg BW) and were returned to their home cages after recovery from anesthesia.

In a separate follow-up experiment, CTB was iontophoresed unilaterally as described above, but with the tracer delivery site targeting the ventral alBST (instead of PVN) in one adult male rat (from bregma: 0.3 mm posterior, 1.7 mm lateral, and 7.4 mm ventral). The goal was to determine whether neurons within the dorsal alBST [which are known to innervate the ventral alBST (Bienkowski and Rinaman, 2013)] express *GLP1R*, and whether these neurons have a GABAergic or glutamatergic phenotype. The existence of other potential sources of input arising from neurons in other regions at the same rostrocaudal level (i.e., from which intact axonal projections to the ventral alBST could have been maintained in *ex vivo* slices) also was investigated.

Ten to twelve days after CTB delivery into PVN or alBST, rats were anesthetized with a lethal dose of sodium pentobarbital (Fatal Plus, 100 mg/kg; Butler Schein, Columbus, OH) and then transcardially perfused

with physiological saline followed by a fixative solution containing 4% paraformaldehyde, 1.4% lysine and 0.3% sodium metaperiodate in 0.1 M sodium phosphate buffer (McLean and Nakane, 1974). Brains were extracted from the skull, blocked and postfixed overnight at 4°C, and cryoprotected in 20% sucrose solution for 24–72 h. Brains were then sectioned coronally (35 μm) using a freezing sliding microtome. Sections were collected sequentially into six adjacent sets and stored in cryopreservant solution (Watson et al., 1986) at −20°C for subsequent processing.

2.4.2. Dual immunocytochemistry and in situ hybridization

Immunofluorescence was combined with RNAscope *in situ* hybridization in order to assess *GLP1R* mRNA expression together with expression of either *Vgat* or *Vglut2* mRNA in retrogradely labeled (i.e., CTB-immunopositive) projection neurons.

RNAscope in situ hybridization: mRNAs were identified using Rn-Glp1r probe (315221, Accession No. NM_012728.1, Target Region: 292–1166), *Vgat* probe (Rn-Slc32a1) and *Vglut2* probe (Rn-Slc17a6), using RNAscope® Multiplex Fluorescent Reagent Kit v2 (323100). Selected tissue sections containing the anterior BST were removed from cryopreservant solution and washed for 1 h in four changes of 0.1M PB. Sections were pretreated with H_2O_2 solution (ACD 322335) for 30 min followed by 4 × 8 min rinses in 0.1M PB. Pretreated sections were then mounted from 0.01M Tris buffer (TB) onto Gold Seal™ UltraStick™ Adhesion Microscope Slides (3039-02; ThermoFisher Scientific, Waltham, MA, USA) and air-dried at room temperature for 1 h. Slides were dipped into 100% ethanol for 10 s and then air-dried for 2–3 h before creating a hydrophobic barrier around each tissue section using a Pap Pen (195506; ThermoFisher Scientific). The barrier was allowed to completely dry at room temperature overnight before proceeding to the next step. Unless otherwise noted, incubations were performed at 40 °C within a HybEZTM Oven, using the HybEZTM Humidity Control Tray. For each section, two to four drops of each reagent solution were used to cover tissue sections, followed by three 3-min rinses in 1 × washing buffer at room temperature. Sections were incubated with Protease IV (322336) for 20–25 min at room temperature, then washed in 0.01M TB four times (1 min/wash). Sections were then incubated in a cocktail of two probes (Rn-Glp1r plus either Rn-Vgat or Rn-Vglut2 for 2 h), followed sequentially by amplification steps with Amp1 (323101) for 30 min, Amp2 (323102) for 30 min, and Apm3 (323103) for 15 min *GLP1R* mRNA and *Vgat* mRNA or *Vglut2* mRNA were then labeled with fluorophore-conjugated Tyramine plus (TSAP) sequentially according to the manufacturer's protocol. For *GLP1R* mRNA, sections were incubated in channel 1-specific HRP (323104) for 15min and Cy3-TSAP (1.5K, tyramine signal amplification plus, NEL744E001KT; PerkinElmer Waltham, MA, USA) for 30 min followed by a 15 min incubation in HRP blocker (323107). Sections were then incubated in channel 2-specific HRP (323105) for *Vgat* mRNA or Vglut2 mRNA for 15 min followed by Cy5-TSAP (1.5K) for 30 min. After a final washing buffer rinse, slides were rinsed in 0.1M PB for 15 min before proceeding to immunofluorescent labeling of CTB.

Immunofluorescent labeling: Incubations were performed at room temperature using the HybEZTM Humidity Control Tray with gentle agitation in a shaker. Sections already processed for RNAscope labeling were incubated in goat anti-CTB antiserum (1:5K, List Biological Labs, cat #703) for 24 h, rinsed for 40 min in 4 changes of 0.1M PB, and then incubated in Alexa 488-conjugated donkey anti-goat secondary antibody (1:400, Jackson ImmunoResearch) for 3 h. After a final rinse in 0.1M PB, sections were air-dried overnight, dehydrated/defatted in graded ethanols and xylene (2 min each), and coverslipped using Cytoseal 60 (VWR).

Image acquisition: Low magnification images were collected using a bright-field and epifluorescent Keyence microscope (catalog #BZ-X700). Higher-resolution images were acquired using a Leica TCS SP8 Confocal Microscope with a 20× air-objective and a 100× oil-objective. Alexa 488 and Cy3 were excited using 488 nm and 552 nm OPSL lasers, respectively, and Cy5 using a 638 nm Diode laser. Confocal images were obtained using Leica LAS version 4.0 image software, with images of each tissue region collected sequentially for each fluorophore to avoid signal contamination. Leica imaging software was used to generate Z plane projections and 3D rotatable maximum intensity projections.

Table 1
Membrane properties of tracer-labeled and non-labeled neurons within the alBST/PS. Values for each property are presented as group mean ± SEM. *Abbreviations:* AHP, afterhyperpolarization; AP, action potential; APT, action potential threshold; RMP, resting membrane potential. *Significantly different, $p < 0.05$ based on two-sample *t*-test, assuming unequal variances.

Property	Tracer-labeled *(# of neurons)*	Non-labeled *(# of neurons)*	T-value	Degrees of freedom
RMP, mV	−58.3 ± 1.3 *(11)*	−57.4 ± 1.2 *(10)*	−0.49	19
APT, mV	−36.8 ± 1.8 *(11)*	−37.8 ± 1.3 *(10)*	0.48	18
AHP amplitude, mV	−13.6 ± 1.6 *(11)*	−10.5 ± 1.2 *(10)*	−1.59	18
Spike frequency, Hz	18.3 ± 2.7 *(11)*	21.2 ± 4.4 *(10)*	−0.55	15
AP amplitude, mV	59.7 ± 0.9 *(11)*	57.4 ± 2.4 *(10)*	0.66	12
AP duration, ms	2.4 ± 0.8 *(11)*	2.0 ± 0.6 *(10)*	1.57	18
Input resistance, MΩ	555.8 ± 51.4 *(12)*	421.6 ± 64.6 *(10)*	1.62	18
Time constant, ms	30.7 ± 3.5* *(12)*	22.1 ± 1.6 *(10)*	2.21	15

3. Results

3.1. Electrophysiological analysis of PVN-projecting neurons in the ventral alBST/PS

Electrophysiological data were collected from PVN-projecting (i.e., tracer-labeled) neurons within the ventral alBST. Given the proximity of the hypothalamic PS to the ventral alBST at rostrocaudal levels used to prepare slices for electrophysiology (see Fig. 1), and given that ventral alBST and PS neurons similarly project to the PVN in rats (Simerly and Swanson, 1988) (Thompson, 2003) (Dong and Swanson, 2006b), we assume that tracer-labeled neurons selected for whole-cell patch-clamp recording included both PS and alBST neurons. Additional recordings were made in non-tracer-labeled alBST/PS neurons located closely adjacent to tracer-labeled neurons. Table 1 summarizes the membrane properties of tracer-labeled and non-labeled neurons recorded before bath application of the specific GLP1R agonist Ex-4 in concentrations ranging from 200 to 600 nM. Despite significant main effects of Ex-4 on the membrane properties of tracer-labeled, PVN-projecting neurons (described below), these effects were independent of Ex-4 concentration. For this reason, data collected from multiple slices and neurons within each experiment are combined in Figs. 1–4, regardless of Ex-4 concentration. In each figure, the Ex-4 concentration used during data collection in individual representative neurons is indicated.

3.1.1. Ex-4 depolarizes the baseline membrane potential of PVN-projecting neurons in the ventral alBST/PS

PVN-projecting neurons in each slice were identified by the presence of red retrobead fluorescent labeling (see Fig. 2H). A subset of labeled neurons in the ventral alBST/PS were selected for whole-cell patch-clamp recording (n = 11 neurons from 7 rats). The membrane properties of bead-labeled neurons before bath application of Ex-4 are reported in Table 1. Only 2 out of 11 neurons displayed spontaneous action potentials.

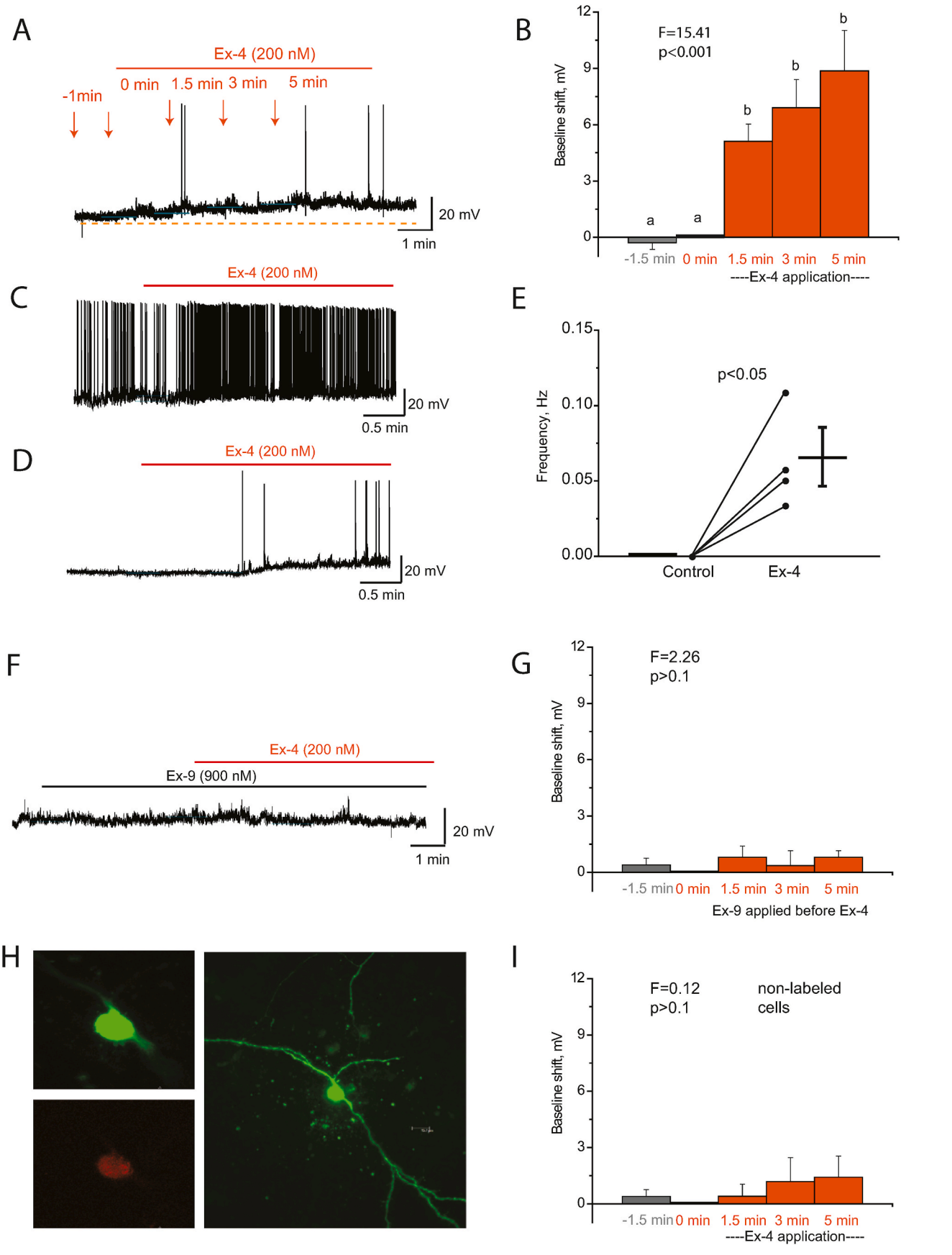

(caption on next page)

Fig. 2. Shift in baseline membrane potential produced by Ex-4.
(A) Baseline recording in a representative PVN-projecting neuron within the anterior vlBST/PS before and after bath application of the specific GLP1R agonist, Ex-4 (200 nM).
(B) Summary data indicating that Ex-4 (200–600 nM) produced a depolarizing shift of the baseline membrane potential in PVN-projecting cells (n = 11 neurons from 7 rats), which was significant from 1.5 to 5 min after bath application.
(C) Baseline recording in a representative PVN-projecting neuron **that displayed** spontaneous firing before Ex-4 (200 nM) application, and increased firing afterwards.
(D) Baseline recording in a representative PVN-projecting neuron that began to fire after Ex-4 (200 nM) application.
(E) Quantification of firing frequency in PVN-projecting neurons (n = 4 neurons from 3 rats) that began to fire after Ex-4 (200 nM) application.
(F) Baseline recording in a representative PVN-projecting neuron before and after bath application of Ex-4 (200 nM) in the presence of 900 nM Ex-9, a specific GLP1R antagonist.
(G) Summary data indicating that Ex-4 (200–600 nM) effects on baseline membrane potential in PVN-projecting neurons (n = 6 cells from 4 rats) are occluded by Ex-9.
(H) A representative PVN-projecting neuron double-labeled with retrobeads (red, bottom left) and Alexa 488 dye (green) applied during neural recording. The same neuron is confocally reconstructed (right panel) to display its morphology.
(I) Ex-4 (200–600 nM) had no effect on baseline membrane potential in non-labeled cells (n = 10 neurons from 5 rats) located in the vicinity of PVN-projecting neurons. (For interpretation of the references to colour in this figure legend, the reader is referred to the Web version of this article.)

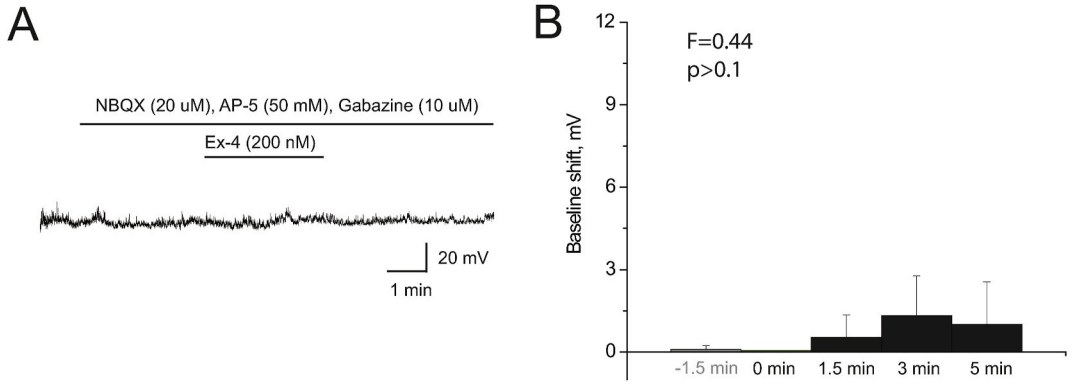

Fig. 3. Synaptic blockers eliminate Ex-4 effects on baseline membrane potential in PVN-projecting neurons.
(A) Baseline recording in a representative PVN-projecting neuron in the anterior vlBST/PS, recorded before and after bath application of Ex-4 (200 nM) in the presence of synaptic blockers.
(B) Summary data indicating that Ex-4 (200–600 nM) effects on baseline membrane potential (n = 10 neurons from 5 rats) were eliminated by prior bath application of synaptic blockers.

We next examined the effect of bath-applied Ex-4 on labeled neurons. One-way ANOVA revealed that Ex-4 produced a substantial upward shift in baseline membrane potential during a 5 min application period, which induced spiking in 3/11 neurons. Compared to baseline membrane potential recorded 1.5 min before and at the time of Ex-4 application, the upward shift was significant at 1.5, 3, and 5 min post-application (Fig. 2A and B). Consistent with the shift in baseline, Ex-4 increased spontaneous firing by 14% and by 100% in the two spontaneously firing neurons (Fig. 2C). Ex-4 also produced firing of action potentials in four additional neurons (Fig. 2D and E; paired comparison; $t = -3.84$; $dF = 3$; $p < 0.05$).

While recording from labeled neurons contained in other slices (n = 6 neurons from 4 rats), we examined whether the depolarizing effect of Ex-4 is mediated through activation of GLP1Rs. For this, the GLP1R antagonist Ex-9 was bath-applied a few minutes before application of Ex-4. While Ex-9 by itself had no effect on baseline membrane potential, it completely occluded the effect of subsequently administered Ex-4 (Fig. 2F and G).

In several slices, whole-cell recordings were made in additional non-labeled neurons that were positioned in close proximity to labeled neurons in the ventral alBST/PS (n = 10 neurons from 5 rats). These nearby non-tracer-labeled neurons possessed intrinsic membrane properties similar to those displayed by labeled neurons; the only documented exception was a significantly slower time constant displayed by tracer-labeled vs. non-labeled neurons (Table 1). Ex-4 failed to generate detectable shifts in baseline membrane potential of non-labeled neurons during the 5-min application period (Fig. 2I).

3.1.2. Synaptic blockers eliminate Ex-4 depolarizing effects on membrane potential

To determine whether Ex-4-induced membrane depolarization is due to effects on the intrinsic membrane properties of PVN-projecting neurons within the ventral alBST/PS (n = 10 neurons from 5 rats), Ex-4 was applied a few minutes after bath application of synaptic blockers. For this, AMPA and kainate receptors were blocked with NBQX, NMDA receptors were blocked with AP-5, and $GABA_A$ receptors were blocked with gabazine. Under these conditions of synaptic blockade, Ex-4 did not significantly alter baseline membrane potential in recorded neurons (Fig. 3A and B). Thus, the depolarizing effect of Ex-4 on PVN-projecting neurons (Fig. 2) depended on modulation of their presynaptic inputs, rather than directly affecting intrinsic ion channel conductances.

3.1.3. Ex-4 reduces inhibitory inputs to PVN-projecting neurons in the ventral alBST/PS

To assess Ex-4 effects on inhibitory responses in PVN-projecting neurons, sIPSCs were recorded in voltage-clamp mode at a holding potential of +12 mV in the presence of NBQX and AP-5 to block glutamatergic receptor signaling. Subsequent bath application of Ex-4 significantly reduced both the frequency and amplitude of sIPSCs recorded in PVN-projecting neurons (n = 7 neurons from 4 rats; Fig. 4A, B, 4C). These sIPSCs could result from action potential-dependent network activity within the slice, and/or action potential-independent transmitter release from presynaptic terminals. To evaluate these possibilities, TTX was applied to block voltage-gated Na^+ channels (and hence, neural firing) within the slice, leaving only action potential (network)-independent mIPSCs. The frequency of mIPSCs represents

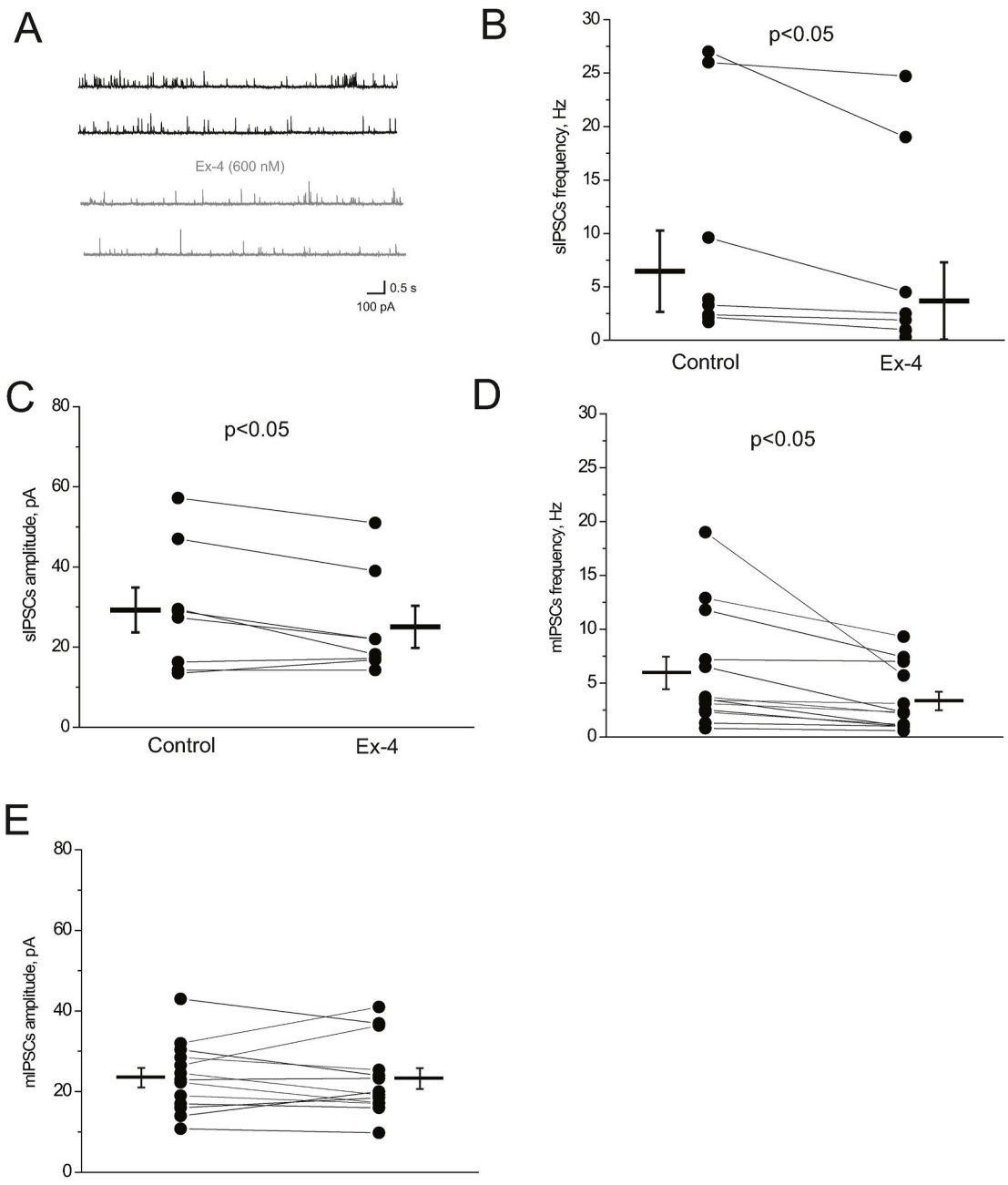

Fig. 4. Ex-4 reduces inhibitory inputs to PVN-projecting neurons.
(A) sIPSCs recorded in a representative PVN-projecting neuron in the anterior vlBST/PS before (top traces) and after (bottom traces) bath application of 600 nM Ex-4.
(B) Summary data indicating that Ex-4 decreased sIPSC frequency in PVN-projecting neurons (n = 7 neurons from 4 rats).
(C) Summary data indicating that Ex-4 decreased sIPSC amplitude in the same PVN-projecting neurons.
(D) In the presence of TTX, Ex-4 decreased mIPSC frequency but not mIPSC amplitude **(E)** in PVN-projecting neurons (n = 13 neurons from 6 rats).

presynaptic GABA release, whereas mIPSC amplitude is a property of postsynaptic receptors. When PVN-projecting cells were recorded in the presence of TTX (n = 13 neurons from 6 rats), Ex-4 reduced the frequency of mIPSCs (Fig. 4D) but did not change their amplitude (Fig. 4E), supporting a presynaptic effect of Ex-4 to reduce inhibitory GABA input to PVN-projecting neurons.

3.1.4. Ex-4 increases excitatory inputs to PVN-projecting neurons in the ventral alBST/PS

To assess Ex-4 effects on sEPSCs, PVN-projecting neurons were recorded in voltage-clamp mode at a holding potential of −70 mV, a condition under which sIPSCs are undetectable (given the −67 mV reversal potential for $GABA_AR$ responses). When cells were recorded under these conditions (n = 8 neurons from 4 rats), bath-applied Ex-4 increased the frequency but not the amplitude of sEPSCs (Fig. 5A, B, 5C), supporting a presynaptic effect of Ex-4 to increase excitatory inputs to the recorded neurons. To confirm this, TTX was bath-applied to isolate action potential-independent mEPSCs. In PVN-projecting neurons recorded under these conditions (n = 6 cells from 3 rats), Ex-4 altered neither mEPSC frequency (Fig. 5D) nor amplitude (Fig. 5E).

3.2. Molecular phenotyping of projection-specific neurons in the ventral alBST/PS

The slice electrophysiology results described above (Figs. 2–5) indicate that bath-applied GLP1R agonist (i.e., Ex-4) reduced inhibitory

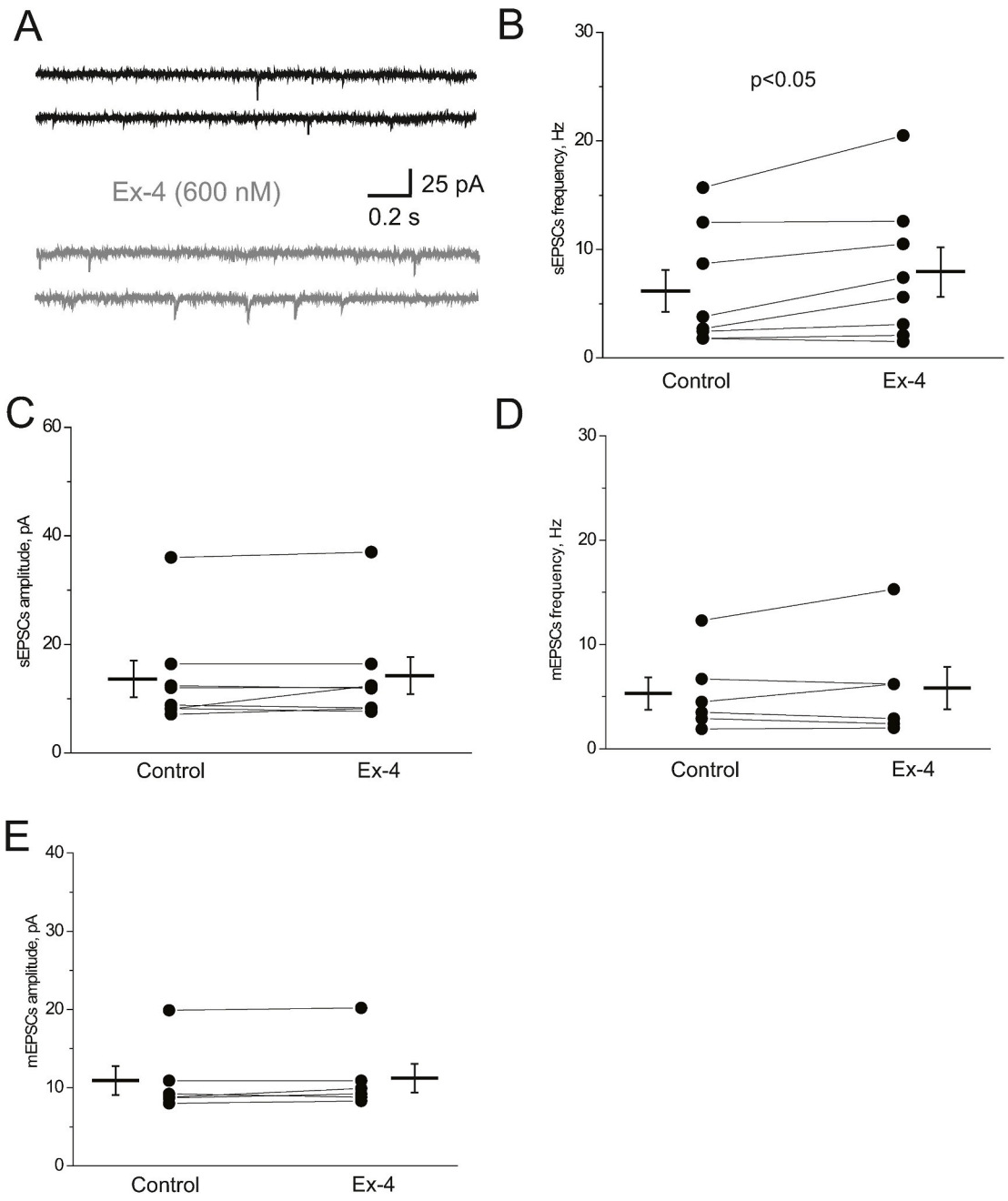

Fig. 5. Ex-4 increases excitatory inputs to PVN-projecting neurons.
(A) sEPSCs recorded in a representative PVN-projecting neuron within the anterior vlBST/PS before (upper trace) and after (lower trace) bath application of 600 nM Ex-4.
(B) Summary data demonstrate that Ex-4 increased sEPSC frequency but not sEPSC amplitude **(C)** in PVN-projecting neurons (n = 8 neurons from 4 rats).
(D) In the presence of TTX, Ex-4 had no significant effect on either mEPSC frequency or mEPSC amplitude **(E).**

inputs and increased excitatory inputs to retrobead-labeled, PVN-projecting neurons within the ventral alBST/PS. Notably, labeled projection neurons recorded in the presence of TTX did not respond directly to Ex-4, suggesting that the majority (and perhaps all) PVN-projecting neurons lack functional GLP1Rs. These results were surprising, because we originally hypothesized that GLP1 would directly activate PVN-projecting neurons in the ventral alBST. To confirm the electrophysiological findings, a separate experiment using a different neural tracer (i.e., CTB) and immunocytochemical amplification of retrograde labeling was conducted to more fully and accurately localize PVN-projecting neurons within the ventral alBST and hypothalamic PS. Next, to examine sources of afferent input to the ventral alBST and to determine whether they express *GLP1R* mRNA, a final follow-up experiment used CTB tracing from the ventral alBST to identify retrogradely-labeled neurons within the dorsal alBST and other regions at the same rostrocaudal level (i.e., likely contained within *ex vivo* slices used for electrophysiological analyses). In each CTB neural tracing experiment, tracer immunolabeling was combined with RNAscope-based *in situ* hybridization to colocalize neural expression of mRNA for *GLP1R* along with *Vgat* or *Vglut2*.

3.2.1. Distribution of PVN-projecting neurons

Following iontophoretic CTB tracer delivery into the hypothalamic PVN, retrogradely-labeled neurons were observed within many distinct

regions of the forebrain and brainstem, consistent with results from previous studies reporting many sources of afferent input to the rat PVN (Sawchenko and Swanson, 1983) (Swanson and Sawchenko, 1980). The present analysis was limited to retrograde labeling in coronal tissue sections through the rostrocaudal level of the anterior BST (i.e., approximately 0.2–0.5 mm caudal to bregma; see Fig. 1), the level at which coronal *ex vivo* slices were taken for electrophysiological recordings in the first experiment. Consistent with previous reports (Dong et al., 2001) (Dong and Swanson, 2006b), CTB-positive neurons occupied ventral alBST regions corresponding to the location of the anteromedial, ventral dorsomedial, fusiform, and anterolateral subnuclei (Figs. 6 and 7). At the more rostral levels included in analysis, an additional prominent cluster of retrogradely-labeled neurons was positioned slightly medial to the ventral alBST, corresponding to the location of the hypothalamic PS (see Fig. 1, lower panel). Unlike the BST, the PS does not receive input from the amygdala, and is thus considered to be part of the hypothalamic preoptic region rather than the BST. However, the PS and ventral alBST share many inputs and outputs, including a

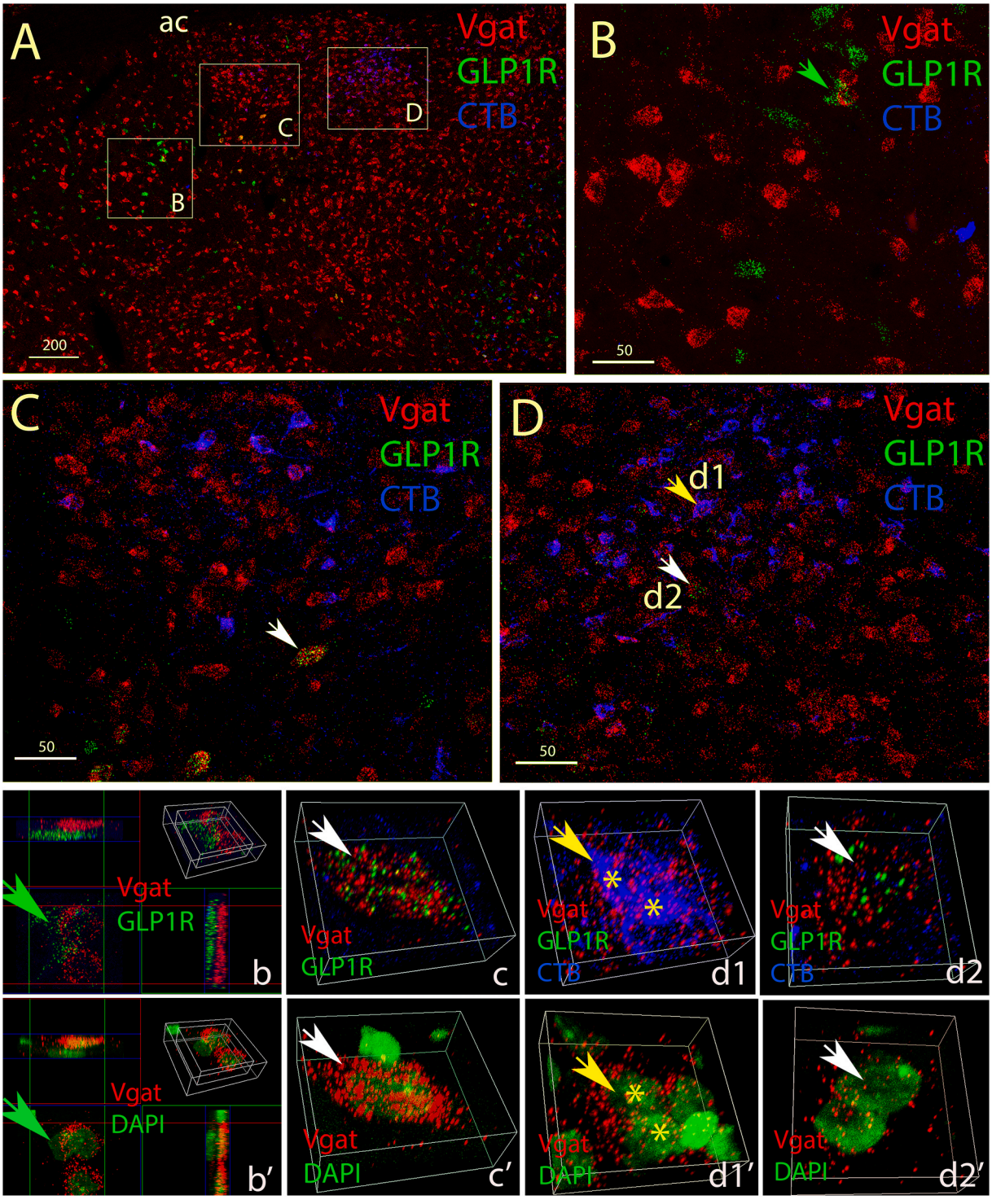

(caption on next page)

Fig. 6. PVN-projecting neurons in the hypothalamic PS and in the ventral anterolateral and fusiform subnuclei of the alBST are predominantly GABAergic and do not express *GLP1R*.

(A) Low magnification Z-max projection image of a coronal section through the ventral alBST (left hemisphere; approximately 0.2 mm caudal to bregma), showing the distribution of PVN-projecting CTB-positive (blue) neurons, neurons expressing *Vgat* mRNA (red), and neurons expressing *GLP1R* mRNA (green). Dorsal is towards the top, medial is towards the right. From lateral to medial, the boxed regions indicated by the labels B, C, and D are shown at higher magnification in the correspondingly labeled panels. ac, anterior commissure. Scale bar, 200 μm.

(B) High magnification Z-max projection image from the most lateral boxed sub-region labeled B in panel A. This region corresponds to the ventrolateral edge of the anterolateral subnucleus of the BST, and also includes a portion of the adjacent substantia innominata. Many neurons in this field of view express *GLP1R* mRNA (green) or *Vgat* mRNA (red), but these two mRNA tags are not colocalized. A few CTB-positive neurons (blue) in the substantia innominata express neither *Vgat* nor *GLP1R* mRNA. The green arrowhead points out two adjacent *Vgat* + neurons depicted at higher magnification in panels b, b', with 3D-MIP (maximum intensity projections). A *GLP1R* + neuron (green) is located adjacent to the two *Vgat*-expressing neurons (red). Panel b' shows the same *Vgat* + cells (red) imaged along with DAPI nuclear label (green).

(C) High magnification Z-max projection image from the boxed sub-region labeled C in panel A, corresponding to a region containing the fusiform subnucleus of the BST. CTB labeling (blue) is imaged along with *Vgat* mRNA (red) and *GLP1R* mRNA (green). Many CTB-positive neurons are visible, all of which express *Vgat* mRNA. However, no CTB-labeled cells in this region express *GLP1R* mRNA. Several *GLP1R* + neurons are present within the lower (more ventral) region in this field of view; most of these express *Vgat* mRNA. The white arrowhead in panel C points out a cell shown at higher magnification in panels c, c', with 3D-MIP to demonstrate colocalization of *Vgat* and *GLP1R* mRNAs (c) and *Vgat* mRNA/DAPI (c').

(D) High magnification Z-max projection image from the most medial boxed sub-region labeled D in panel A, corresponding to the location of the hypothalamic PS. CTB labeling (blue) is imaged along with *Vgat* mRNA (red) and *GLP1R* mRNA (green). At this rostrocaudal level of the PS, most CTB-labeled neurons express *Vgat* mRNA, but none were observed to express *GLP1R* mRNA. Most of the *GLP1R* + neurons visible within this region were observed to express *Vgat* mRNA. The yellow arrowhead (labeled d1) points out two CTB-positive cells shown at higher magnification in panel d1 (asterisks) with 3D-MIP to demonstrate their colocalization of *Vgat* mRNA (red). Panel d1′ shows the same field of view with *Vgat* mRNA labeling (red) imaged along with nuclear DAPI (green). The white arrowhead in panel D (labeled d2) indicates two non-tracer-labeled neurons, shown at higher magnification (3D-MIP) in panel d2 to demonstrate cellular colocalization of *Vgat* (red) and *GLP1R* mRNA (green). Intracellular colocalization of both mRNA labels is demonstrated in panel d2′, in which *Vgat* mRNA (red) is imaged along with nuclear DAPI (green). (For interpretation of the references to colour in this figure legend, the reader is referred to the Web version of this article.)

prominent projection to the PVN (Simerly and Swanson, 1988) (Thompson, 2003) (Dong and Swanson, 2006b). CTB-positive neurons also were present within the substantia innominata, and throughout the median preoptic and anteroventral periventricular nuclei of the anterior hypothalamus. It should be noted that tracer-labeled neurons in these locations were not included in *ex vivo* slice electrophysiology, because their positions did not meet the selection criteria (i.e., not close to the anterior commissure, not vertically aligned with the lateral ventricle).

3.2.3. PVN-projecting neurons in the hypothalamic PS and ventral alBST are predominantly or exclusively GABAergic, and very few express GLP1R

CTB immunofluorescence was combined with fluorescent RNAscope *in situ* hybridization to colocalize retrograde labeling with *GLP1R* mRNA and *Vgat* mRNA, the latter to identify GABAergic neurons. Alternate sections from the same animals were processed to colocalize CTB, *GLP1R* mRNA, and *Vglut2* mRNA, the latter to identify glutamatergic neurons. In each section analyzed, retrogradely-labeled (CTB-positive) neurons in different subnuclei of the ventral alBST and adjacent regions were inspected at low and high magnification to discern co-expression of mRNA for *GLP1R* and either *Vgat* or *Vglut2* mRNA.

Essentially all CTB-positive, PVN-projecting neurons within the fusiform, anterolateral, and anteromedial subnuclei of the ventral alBST and within the adjacent hypothalamic PS were GABAergic, based on visible labeling for *Vgat* mRNA (Fig. 6) and/or lack of *Vglut2* mRNA labeling (Fig. 7). Quantitative analyses based on high-magnification (100×) confocal imaging of individual CTB-positive neurons confirmed that 100% (i.e., 66/66 cells) expressed *Vgat* mRNA in sections processed for *Vgat*, whereas only 1.5% (1/66) expressed *Vglut2* mRNA in sections processed for *Vglut2*. Surprisingly, only 4.5% of PVN-projecting neurons within the PS nucleus and ventral alBST expressed mRNA for *GLP1R* (i.e., 6/132 CTB-positive neurons). All six of these neurons were identified in tissue sections processed to localize *Vglut2* mRNA, and were located in regions corresponding to the anteromedial and dorsomedial subnuclei of the ventral alBST (Fig. 7). Only one of these CTB-positive, *GLP1R*-expressing neurons expressed *Vglut2* mRNA, suggesting that the other five cells were GABAergic. However, 0% of CTB-positive neurons (i.e., 0/66) expressed *GLP1R* in adjacent sections processed to localize *Vgat* mRNA. Regarding *GLP1R*-expressing neurons within the PS nucleus and ventral alBST that were imaged at high magnification, approximately 58% (i.e., 14/24) co-expressed *Vgat* mRNA in sections processed for *Vgat* (Fig. 6), and approximately 6.9% (i.e., 2/29) expressed *Vglut2* mRNA in sections processed for *Vglut2* (Fig. 7).

3.2.3. GLP1R is expressed by a subset of GABAergic neurons in the oval subnucleus of the dorsal alBST and glutamatergic neurons in substantia innominata that innervate the ventral alBST/PS

Consistent with previous reports (Dong et al., 2001) (Shin et al., 2008) (Bienkowski and Rinaman, 2013), iontophoretic delivery of CTB into the ventral alBST/PS produced retrograde labeling that was concentrated within the oval subnucleus of the dorsal alBST at the same rostro-caudal level (Fig. 8). High-magnification (100×) confocal imaging of CTB-positive neurons within the oval subnucleus confirmed that 96.9% were GABAergic (i.e., 31/32 cells), based on expression of *Vgat* mRNA (Fig. 8). A small subset (i.e., 6.3%; 2/32) of these tracer-labeled neurons co-expressed mRNA for both *Vgat* and *GLP1R* (Fig. 8).

Additional scattered retrogradely-labeled neurons were observed in the hypothalamic medial preoptic nucleus (MPN) and median preoptic area (MePO), and also within the substantia innominata (SI) in coronal sections through the same rostrocaudal level (i.e., representing network inputs that could have been preserved in *ex vivo* slices used for electrophysiological data collection). All or most CTB-positive neurons in the MPN (i.e., 100%; 7/7 CTB + cells), MePO (100%; 20/22 cells), and SI (55.5%; 5/9 cells) expressed *Vglut2* mRNA. Of these, three tracer-labeled cells expressed *GLP1R* mRNA; these were located in SI, and they co-expressed *Vglut2 (i.e., 33% of CTB-labeled SI neurons; 3/9 cells)*.

4. Discussion

We previously reported that ventral alBST neurons that express *GLP1R* are predominantly GABAergic in rats, and that virally-mediated "knock-down" of *GLP1R* expression in the alBST prolongs the plasma cort response to acute stress (Zheng et al., 2019). Based on evidence that a GABAergic projection pathway from ventral alBST to PVN serves to limit stress-induced activation of the HPA axis in rats (Radley et al., 2009) (Johnson et al., 2016), we hypothesized that the GABAergic neurons comprising this projection pathway are directly stimulated by GLP1. Results from the present study are consistent with the functional component of our hypothesis, but they challenge a specific detail. As predicted, pharmacological stimulation of GLP1R's in *ex vivo* slices through the rat alBST promoted depolarization of identified PVN-projecting GABAergic neurons. However, with rare exception, PVN-projecting neurons within the ventral alBST did not express *GLP1R*

mRNA, consistent with electrophysiological data indicating that the net excitatory effect of GLP1 signaling on these PVN-projecting neurons is indirect, and due to circuit-mediated effects within the *ex vivo* slice that increase excitatory synaptic inputs to the recorded neurons, coupled with circuit-independent effects that decrease inhibitory synaptic inputs. We do not believe that retrograde labeling prevented detection of *GLP1R* mRNA expression in PVN-projecting neurons, because CTB-positive, *GLP1R* mRNA-expressing neurons were observed within the oval subnucleus of the dorsal alBST and within the SI after tracer injection into the ventral alBST. We also have documented that RNAscope tissue processing does not reduce or otherwise interfere with subsequent CTB immunolabeling (data not shown). Nevertheless, our ability to visualize double-labeled cells (i.e., CTB + cells that express *GLP1R* mRNA) via confocal microscopy likely underestimates their true presence within each analyzed region.

Whole-cell patch recordings in tracer-labeled neurons likely included cells within the hypothalamic PS, positioned immediately adjacent to the ventral alBST. The PS is not considered a component of the BST, because it does not receive axonal input from the amygdala (Ju and Swanson, 1989). However, the cytoarchitectural, connectional, and

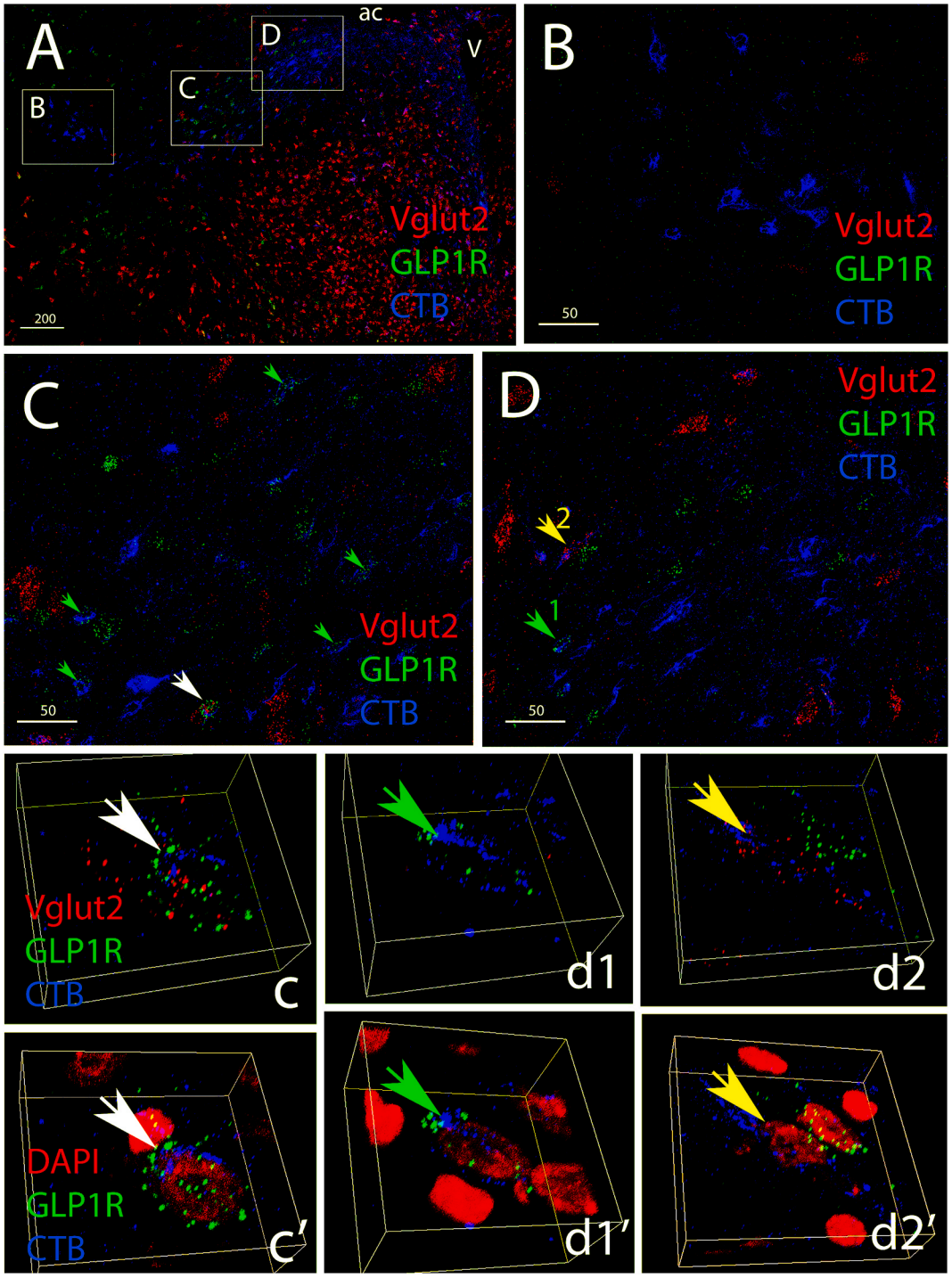

(caption on next page)

Fig. 7. PVN-projecting neurons in the ventral alBST do not express *Vglut2*; PVN-projecting neurons in the anteromedial subnucleus rarely express *GLP1R* mRNA.

(A) Low magnification Z-max projection image of a coronal section through the caudal portion of the left ventral alBST, approximately 0.5 mm caudal to bregma. Dorsal is towards the top, medial is towards the right. CTB labeling (blue) is imaged together with *GLP1R* mRNA (green) and *Vglut2* mRNA (red). The boxed regions indicated by the labels B, C, and D (from lateral to medial) are shown at higher magnification in the correspondingly labeled panels. More medially (closer to the third ventricle), CTB-labeled neurons occupy the median preoptic and preoptic periventricular nuclei of the hypothalamus. ac, anterior commissure; V, third ventricle. Scale bar, 200 μm.

(B) High magnification Z-max projection image from the boxed sub-region labeled B in panel A, corresponding to the location of the ventral anterolateral and rhomboid subnuclei of the BST. CTB-labeled neurons in this region do not express mRNA for *Vglut2*, although a few *Vglut2*-expressing cells are present. Sparse *GLP1R* mRNA expression is not colocalized with CTB.

(C) High magnification Z-max projection image from the boxed sub-region labeled C in panel A, corresponding to the location of the anteromedial subnucleus of the BST. None of the CTB-labeled neurons in this region express *Vglut2* mRNA, but several express *GLP1R* mRNA (confirmed examples of colocalization are indicated by arrowheads). The larger white arrowhead points out a CTB-labeled, *GLP1R* + neuron located adjacent to a different *Vglut2*+ cell. These cells are shown at higher magnification in panel c, where 3D-MIP demonstrates colocalization of CTB (blue) and *GLP1R* mRNA (green) imaged along with *Vglut2* (red). In c', CTB and *GLP1R* mRNA is imaged along with nuclear DAPI (red). Scale bar, 50 μm.

(D) High magnification Z-max projection image from the boxed sub-region labeled D in panel A, corresponding to the location of the dorsomedial subnucleus of the BST; a lateral portion of the hypothalamic median preoptic nucleus also is included in the upper (more dorsal) region of this field of view. Most CTB-positive neurons in this region express neither *Vglut2* nor *GLP1R* mRNA; exceptions include the two neurons indicated by arrowheads. The green arrowhead (1) points out a CTB-labeled neuron that expresses *GLP1R* mRNA [shown in a higher magnification 3D-MIP in d1 (CTB plus *GLP1R*), with red DAPI nuclear labeling added in d1']. The yellow arrowhead (2) points out a CTB-labeled neuron that expresses *Vglut2* but not *GLP1R* mRNA [shown in a higher magnification 3D-MIP in d2 (CTB plus *Vglut2* mRNA are colocalized in the same cell, whereas an adjacent cell expresses *GLP1R* but is not CTB-positive; red DAPI nuclear labeling is included with CTB and *GLP1R* labeling in d2']. (For interpretation of the references to colour in this figure legend, the reader is referred to the Web version of this article.)

neurochemical properties of PS neurons are otherwise quite similar to those of neurons within the ventral alBST (Simerly and Swanson, 1988) (Thompson, 2003) (Dong and Swanson, 2006b). In this regard, results from the present study confirmed that virtually all PVN-projecting neurons within the ventral alBST and PS express *Vgat* mRNA, identifying them as GABAergic. This finding is consistent with previous reports that the majority of neurons within the ventral alBST and PS in rats are GABAergic (Sun and Cassell, 1993). Not surprisingly, virtually all alBST/PS neurons that express mRNA for *GLP1R* were seen to co-express *Vgat* mRNA. This finding is consistent with results from our previous study demonstrating co-expression of mRNA's for *GLP1R* and a different GABAergic marker (i.e., Gad1) in the rat alBST (Zheng et al., 2019).

Data obtained from whole-cell patch recordings in *ex vivo* slices indicated that the intrinsic membrane properties of tracer-labeled (i.e., PVN-projecting) alBST/PS neurons closely resembled the membrane properties of nearby neurons that were not tracer-labeled (Table 1), and were consistent with previous reports describing electrophysiological properties of alBST neurons in rats and mice (Egli and Winder, 2003) (Hammack et al., 2007) (Rodríguez-Sierra et al., 2013) (Williams et al., 2018).

As noted above, the depolarizing effect of Ex-4 on tracer-labeled neurons within the ventral alBST/PS appeared to be due to a reduction in inhibitory (IPSP) inputs coupled with an increase in excitatory (EPSP) inputs. In our experiments, the ability of Ex-4 to reduce IPSC frequency and increase EPSC indicates that Ex-4 reduced presynaptic release of GABA and increased presynaptic release of glutamate onto the recorded PVN-projecting neurons. In the absence of TTX, IPSCs and EPSCs include a mixture of network-dependent and independent events. Conversely, in the presence of TTX, recorded currents (mIPSCs and mEPSCs) are network-independent, but still potentially modulated by factors (e.g., Ex-4) that directly alter presynaptic release of GABA and/or glutamate onto recorded neurons. The ability of Ex-4 to reduce the frequency of network-independent IPSCs was preserved in the presence of TTX, whereas the ability of Ex-4 to increase EPSC frequency was abolished. As schematized in Fig. 9, these data support the view that recorded PVN-projecting neurons receive inhibitory input from presynaptic axon terminals that respond directly to Ex-4 by reducing network-independent GABA release, and that the same PVN-projecting neurons receive excitatory input from terminals that increase glutamate release as a network-mediated response to Ex-4. Sources of synaptic input to the recorded PVN-projecting neurons may include other local neurons within the anterior vlBST that express *GLP1R* mRNA, although patch recordings made in non-tracer-labeled neurons located in close proximity to PVN-projecting neurons failed to identify any that responded (either directly or indirectly) to bath-applied Ex-4. It is possible that increased sampling of non-labeled neurons would have revealed some that responded to Ex-4.

Additional projection pathways that were likely preserved within coronal *ex vivo* slices arise from the oval subnucleus of the dorsal alBST, the hypothalamic MPO and MePO, and the SI. Each of these regions reportedly contains cells that express *GLP1R* mRNA (Merchenthaler et al., 1998), with the oval subnucleus providing an especially robust input to the subjacent ventral alBST (Dong et al., 2001) (Shin et al., 2008). In our final follow-up experiment, we combined *in situ* hybridization with retrograde labeling to reveal that neurons within the oval subnucleus that project to the ventral alBST are GABAergic, and that a small proportion of these neurons express *GLP1R* mRNA. We also found scattered retrogradely-labeled neurons within the SI and hypothalamic MPO and MePO at the same rostrocaudal level as the ventral alBST. Most of these tracer-labeled neurons expressed *Vglut2* mRNA, making them candidates for the observed network-dependent increase in excitatory input to PVN-projecting neurons. Indeed, a subset of tracer-labeled neurons (in SI) co-expressed *GLP1R* and *Vglut2* mRNA. It is likely that the network-mediated effect of Ex-4 to increase presynaptic glutamate release onto recorded PVN-projecting neurons within *ex vivo* slices also included effects that were indirect. It also is possible that the effect is mediated by the small population of *Vglut2*-and *GLP1R*-expressing neurons that we observed within the ventral alBST, but whose identification as a source of presynaptic input to PVN-projecting neurons was obscured within the tracer injection site. These observations are summarized in Fig. 9.

As mentioned above, compared to input from scattered neurons within the hypothalamus and SI, the oval subnucleus of the dorsal alBST provided robust input to the ventral alBST. In mice, activation of oval BST neurons leads to *inhibition* of postsynaptic ventral alBST neurons that project to the lateral hypothalamic area (Wang et al., 2019); this population of ventral alBST neurons may be distinct from those that project to the PVN. Our finding that bath application of Ex-4 promotes *depolarization* of PVN-projecting alBST/PS neurons suggests that potential GLP1R-mediated effects on GABAergic inputs from the oval subnucleus contribute to disinhibition of PVN-projecting alBST/PS neurons. For example, GLP1R signaling could inhibit the GABAergic oval-to-ventral alBST projection, and/or could activate oval GABAergic neurons that synapse on another group of inhibitory interneurons that are presynaptic to PVN-projecting neurons in the ventral alBST. In this regard, GLP1R signaling in the mouse alBST directly depolarizes or hyperpolarizes different subpopulations of dorsal and ventral alBST neurons that apparently are intermixed (Williams et al., 2018), evidence

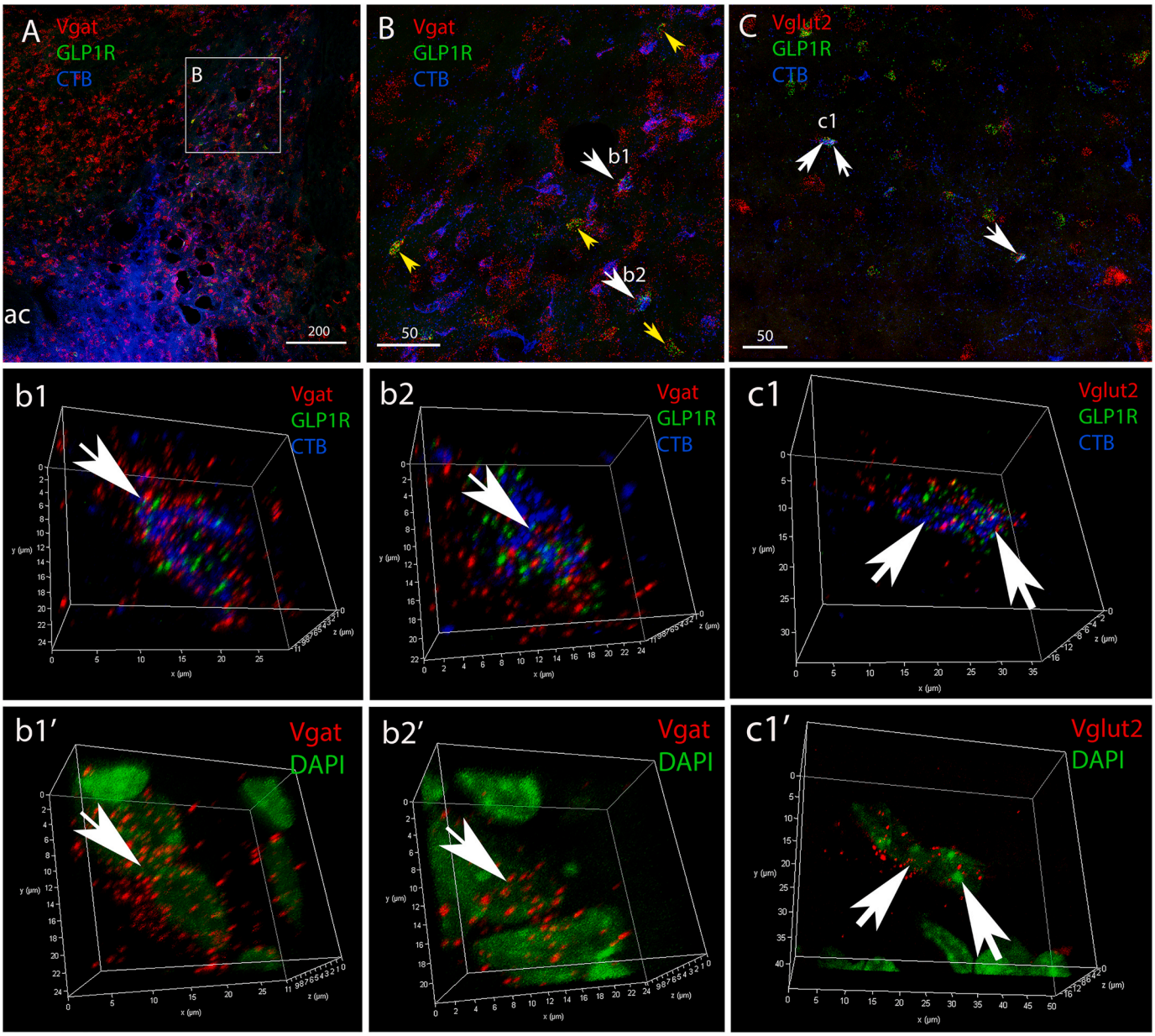

Fig. 8. Sources of *GLP1R*-expressing GABAergic and glutamatergic input to the ventral alBST.
(A) Z-max projection image of a coronal section through the caudal portion of the right alBST, approximately 0.15 mm caudal to bregma. Dorsal is towards the top, medial is towards the left. The CTB iontophoretic tracer delivery site (lower part of image, adjacent to the ac) is centered in a region corresponding to the location of the ventral anteromedial, fusiform, and anterolateral subnuclei of the BST. CTB labeling (blue) is visible both within the injection site and retrogradely transported to the dorsal alBST. CTB labeling is imaged together with mRNA for *Vgat* (red) and *GLP1R* (green). The boxed region labeled B corresponds to the oval subnucleus of the dorsal alBST, shown at higher magnification in the correspondingly labeled panel. ac, anterior commissure. Scale bar, 200 μm.
(B) Higher magnification Z-max projection image from the boxed sub-region labeled B in panel A, corresponding to the oval subnucleus of the dorsal alBST. All CTB-positive neurons (blue) express *Vgat* mRNA (red), and several also express *GLP1R* mRNA (green). In addition, many non-tracer-labeled neurons express *Vgat* mRNA, and some of these co-express *GLP1R* mRNA (indicated by small yellow arrowheads). The larger white arrowheads labeled b1 and b2 point out two triple-labeled neurons (i.e., positive for CTB, *Vgat* mRNA, and *GLP1R* mRNA). These cells are shown at higher magnification in 3D-MIP images in panels b1 and b2. For each cell, colocalization of all three labels is demonstrated in b1′ and b2′, which depict *Vgat* mRNA (red) and nuclear DAPI label (green). Scale bar, 50 μm.
(C) Higher magnification Z-max projection image through the substantia innominata (SI), approximately 0.15 mm caudal to bregma. Most CTB-positive neurons (blue) express *Vglut2* mRNA (red), and a subset of these express *GLP1R* mRNA (green). The white arrowheads point out three triple-labeled neurons (i.e., positive for CTB, *Vglut2* mRNA, and *GLP1R* mRNA). Two of these cells (c1) are shown at higher magnification in 3D-MIP images in panel c1. For each cell, colocalization of all three labels is demonstrated in c1; in c1′, *Vglut2* mRNA (red) is imaged together with nuclear DAPI (green). Scale bar, 50 μm. (For interpretation of the references to colour in this figure legend, the reader is referred to the Web version of this article.)

that coupling to G_S protein (Fletcher et al., 2016) is not obligatory for all GLP1R-mediated neural responses [see also (Cork et al., 2015) (Ong et al., 2017) (Smith et al., 2019)]. In addition, GLP1R protein within the BST and other brain regions is often localized in the membrane of axon varicosities and terminals, consistent with a presynaptic modulatory action of GLP1 signaling (Farkas et al., 2020). Consistent with this, our results indicate that Ex-4 reduced IPSCs recorded in PVN-projecting neurons in a network-independent manner, perhaps due to a direct GLP1R-mediated effect to reduce GABA release from presynaptic terminals (Fig. 9).

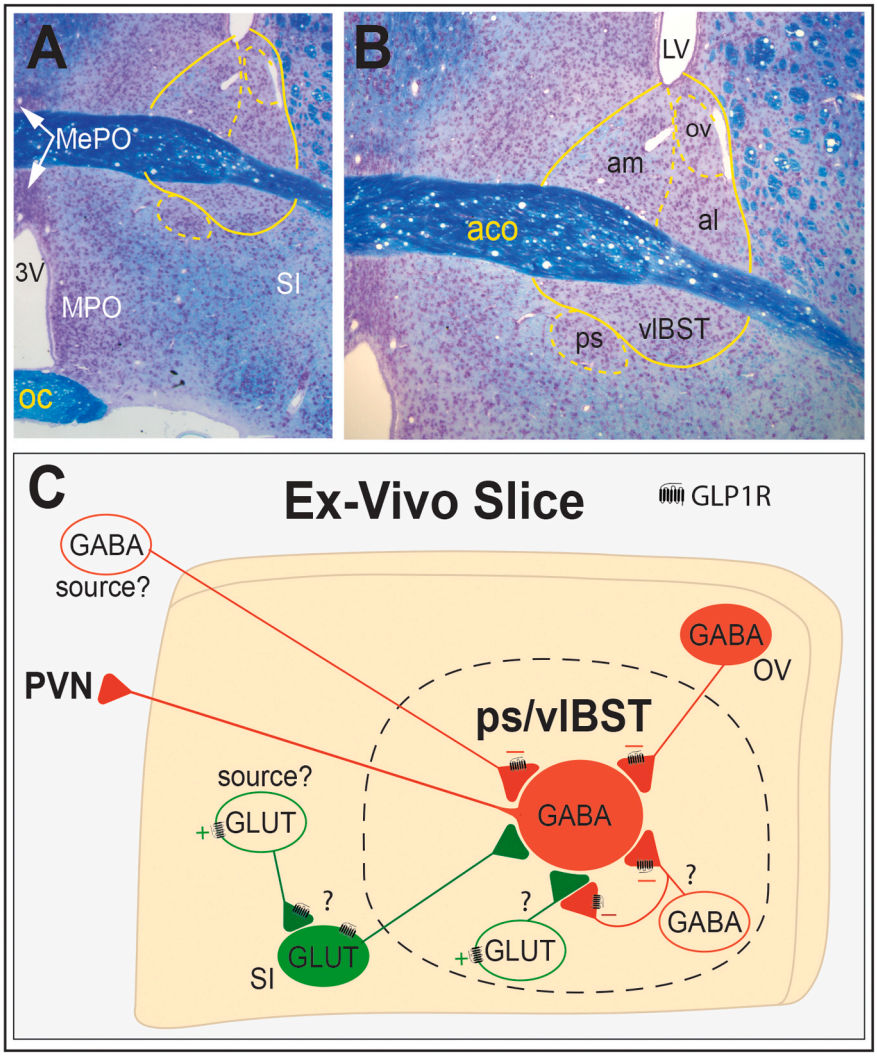

Fig. 9. Summary schematic of key findings and open questions regarding the ability of bath-applied Ex-4 to activate ventral alBST neurons that project to the PVN.

(A) Low-magnification view of a Klüver-Barrera-stained coronal tissue section through the anterior BST, in which the locations of the SI and hypothalamic MePO and MPO at the same rostrocaudal level are indicated.

(B) Higher-magnification view of the same section, in which the oval nucleus (ov) and other BST nuclei are labeled.

(C) Model schematic representing results from *ex-vivo* slice recording, retrograde tracing, and *in situ* hybridization. Neurons within the ps/anterior vlBST that project to the PVN are GABAergic (*Vgat*+), do not express *GLP1R* mRNA (with rare exception), and are indirectly depolarized by bath-applied GLP1R agonist (Ex-4). Given that these responses include network-independent reductions in IPSC frequency, bath-applied Ex-4 may bind to inhibitory-type GLP1R's on presynaptic GABAergic terminals to thereby reduce GABA release directly onto PVN-projecting neurons, and potentially also to disinhibit glutamate release onto PVN-projecting neurons. Ex-4-sensitive GABAergic inputs could originate from neurons in the oval nucleus, vlBST, and/or locations external to the slice. Bath-applied Ex-4 also increased the frequency of EPSCs recorded in PVN-projecting neurons in a network-dependent manner that was blocked by TTX, evidence that Ex-4 increased glutamatergic inputs from neurons contained within the slice; as noted above, this effect could include presynaptic disinhibition of glutamate release. Scattered glutamatergic (*Vglut2*+) inputs to the ps/vlBST arose from the MePO, MPO, and SI, and a subset of tracer-labeled SI neurons co-expressed *Vglut2* and *GLP1R* mRNA. Other potential sources of glutamatergic input to PVN-projecting neurons include *Vglut2*+ neurons within the vlBST that co-express *GLP1R* mRNA. Glutamatergic inputs to PVN-projecting neurons also may be activated by Ex-4 in a network-dependent manner, even if the inputs themselves do not express *GLP1R* mRNA. 3V, third ventricle; aco, anterior commissure; al, anterolateral subnucleus; am, anteromedial subnucleus; LV, lateral ventricle, oc, optic chiasm; ps, parastrial nucleus.

To our knowledge, the current report is the first to examine GLP1R-mediated effects on the physiological properties of BST neurons with identified axonal projections. Previous studies conducted in rats and mice have reported a diversity of modulatory effects mediated by GLP1R signaling across different brain regions. For example, GLP1R signaling within the rat dorsomedial hypothalamus (DMH) appears to activate local GABAergic interneurons (Lee et al., 2018). Conversely, GLP1R signaling appears to exert a net inhibitory effect on GABAergic neurons within the mouse dorsolateral septum, where neurons become more excitable after genetic ablation of *GLP1R* (Harasta et al., 2015). Other studies have reported that GLP1R signaling reduces the excitability of neurons within the paraventricular thalamic nucleus that project to the nucleus accumbens, and that this effect is mediated in part via suppression of excitatory synaptic drive (Ong et al., 2017). On the other hand, GLP1R signaling enhances membrane trafficking of glutamate AMPA receptor subunits to thereby increase postsynaptic excitatory synaptic transmission within mouse PVN neurons (Liu et al., 2017). The latter finding suggests a potential mechanism underlying the increased excitatory postsynaptic currents that we recorded in ventral alBST neurons that project to the PVN; however, and in contrast to our current findings in rat alBST neurons, inhibitory postsynaptic currents were not altered by GLP1R signaling in mouse PVN neurons (Liu et al., 2017). The collective data support the view that GLP1R-mediated neural responses display a high degree of heterogeneity across different brain regions. Additional complexity arises from heterogeneity among neurons within each brain region; for example, ventral alBST/PS neurons that project to the PVN in rats are distinct from an intermingled population of midbrain-projecting neurons (Johnson et al., 2019), and it is possible that GLP1R signaling differentially impacts these distinct projections.

In summary, results from the present study provide evidence that *GLP1R* is not expressed by the large majority of PVN-projecting neurons within the ventral alBST in rats. However, GLP1R-mediated effects on presynaptic inputs to these GABAergic neurons consistently promoted their depolarization. Considered together with results from previous studies (Radley et al., 2009) (Johnson et al., 2016) (Zheng et al., 2019), our findings reveal a potential GLP1R-mediated mechanism through which the ventral alBST exerts inhibitory control over the endocrine HPA axis. Additional research is necessary to unravel the potentially complex neural circuitry through which GLP1 neurons in the caudal brainstem engage GLP1R signaling pathways to exert this modulatory control, and the physiological conditions under which these circuits are engaged.

Funding

This work was supported by the National Institutes of Health [grant number MH059911 to L.R.].

CRediT authorship contribution statement

Nadya Povysheva: Writing – original draft, Methodology, Validation, Formal analysis, Investigation, Visualization. **Huiyuan Zheng:** Writing – review & editing, Methodology, Validation, Formal analysis, Investigation, Visualization. **Linda Rinaman:** Conceptualization, Methodology, Writing – original draft, Writing – review & editing, Supervision, Project administration, Funding acquisition.

Declaration of competing interest

The authors have no competing interests to declare.

Acknowledgments

We thank Alissa DePiro for assistance with confocal reconstructions, and Dr. J. Patrick Card for helping to create the summary diagram (Fig. 9).

References

Bienkowski, M.S., Wendel, E.S., Rinaman, L., 2013. Organization of multisynaptic circuits within and between the medial and central extended amygdala. J. Comp. Neurol. 521, 3406–3431.

Cork, S.C., Richards, J.E., Holt, M.K., Gribble, F.M., Reimann, F., Trapp, S., 2015. Distribution and characterisation of Glucagon-like peptide-1 receptor expressing cells in the mouse brain. Mol Metab 4, 718–731.

Crestani, C.C., Alves, F.H., Gomes, F.V., Resstel, L.B., Correa, F.M., Herman, J.P., 2013. Mechanisms in the bed nucleus of the stria terminalis involved in control of autonomic and neuroendocrine functions: a review. Curr. Neuropharmacol. 11, 141–159.

Dong, H.-W., Swanson, L.W., 2006a. Projections from bed nuclei of the stria terminalis, anteromedial area: cerebral hemisphere integration of neuroendocrine, autonomic, and behavioral aspects of energy balance. J. Comp. Neurol. 494, 142–178.

Dong, H.-W., Swanson, L.W., 2006b. Projections from bed nuclei of the stria terminalis, dorsomedial nucleus: implications for cerebral hemisphere integration of neuroendocrine, autonomic, and drinking responses. J. Comp. Neurol. 494, 75–107.

Dong, H.-W., Petrovich, G.D., Watts, A.G., Swanson, L.W., 2001. Basic organization of projections from the oval and fusiform nuclei of the bed nuclei of the stria terminalis in adult rat brain. J. Comp. Neurol. 436, 430–455.

Egli, R.E., Winder, D.G., 2003. Dorsal and ventral distribution of excitable and synaptic properties of neurons of the bed nucleus of the stria terminalis. J. Neurophysiol. 90, 405–414.

Farkas, E., Szilvásy-Szabó, A., Ruska, Y., Sinkó, R., Grønbech Rasch, M., Egebjerg, T., Pyke, C., Gereben, B., Bjerre Knudsen, L., Fekete, C., 2020. Distribution and ultrastructural localization of the glucagon-like peptide-1 receptor (GLP-1R) in the rat brain. Brain Struct. Funct. 226, 225–245.

Fletcher, M.M., Halls, M.L., Christopoulos, A., Sexton, P.M., Wootten, D., 2016. The complexity of signalling mediated by the glucagon-like peptide-1 receptor. Biochem. Soc. Trans. 44, 582–588.

Goke, R., Fehmann, H.C., Linn, T., Schmidt, H., Krause, M., Eng, J., Goke, B., 1993. Exendin-4 is a high potency agonist and truncated exendin-(9-39)-amide an antagonist at the glucagon-like peptide 1-(7-36)-amide receptor of insulin-secreting beta-cells. J. Biol. Chem. 268, 19650–19655.

Guide for the Care and Use of Laboratory Animals, eighth ed., 2011. National Academies Press, Washington, D.C. Available at: http://www.nap.edu/catalog/12910.

Hammack, S., Mania, I., Rainnie, D.G., 2007. Differential expression of intrinsic membrane currents in defined cell types of the anterolateral bed nucleus of the stria terminalis. J. Neurophysiol. 98, 638–656.

Harasta, A.E., Power, J.M., von Jonquieres, G., Karl, T., Drucker, D.J., Housley, G.D., Schneider, M., Klugmann, M., 2015. Septal glucagon-like peptide 1 receptor expression determines suppression of cocaine-induced behavior. Neuropsychopharmacology 40, 1969–1978.

Heppner, K.M., Kirigiti, M., Secher, A., Paulsen, S.J., Buckingham, R., Pyke, C., Knudsen, L.B., Vrang, N., Grove, K.L., 2015. Expression and distribution of glucagon-like peptide-1 receptor mRNA, protein and binding in the male nonhuman primate (Macaca mulatta) brain. Endocrinology 156, 255–267.

Holt, M.K., Trapp, S., 2016. The physiological role of the brain GLP-1 system in stress. Cogent. Biol. 2, 1229086.

Holt, M.K., Richards, J.E., Cook, D.R., Brierley, D.I., Williams, D.L., Reimann, F., Gribble, F.M., Trapp, S., 2019. Preproglucagon neurons in the nucleus of the solitary tract are the main source of brain GLP-1, mediate stress-induced hypophagia, and limit unusually large intakes of food. Diabetes 68, 21–33.

Johnson, S.B., Emmons, E.B., Anderson, R.M., Glanz, R.M., Romig-Martin, S.A., Narayanan, N.S., LaLumiere, R.T., Radley, J.J., 2016. A basal forebrain site coordinates the modulation of endocrine and behavioral stress responses via divergent neural pathways. J. Neurosci. 36, 8687–8699.

Johnson, S.B., Emmons, E.B., Lingg, R.T., Anderson, R.M., Romig-Martin, S.A., LaLumiere, R.T., Narayanan, N.S., Viau, V., Radley, J.J., 2019. Prefrontal–bed nucleus circuit modulation of a passive coping response set. J. Neurosci. 39, 1405–1419.

Ju, G., Swanson, L.W., 1989. Studies on the cellular architecture of the bed nuclei of the stria terminalis in the rat: I. cytoarchitecture. J. Comp. Neurol. 280, 587–602.

Kinzig, K.P., D'Alessio, D.A., Herman, J.P., Sakai, R.R., Vahl, T.P., Figueiredo, H.F., Murphy, E.K., Seeley, R.J., 2003. CNS glucagon-like peptide-1 receptors mediate endocrine and anxiety responses to interoceptive and psychogenic stressors. J. Neurosci. 23, 6163–6170.

Lee, S.J., Sanchez-Watts, G., Krieger, J.-P., Pignalosa, A., Norell, P.N., Cortella, A., Pettersen, K.G., Vrdoljak, D., Hayes, M.R., Kanoski, S.E., Langhans, W., Watts, A.G., 2018. Loss of dorsomedial hypothalamic GLP-1 signaling reduces BAT thermogenesis and increases adiposity. Mol Metab 11, 33–46.

Liu, J., Conde, K., Zhang, P., Lilascharoen, V., Xu, Z., Lim, B.K., Seeley, R.J., Zhu, J.J., Scott, M.M., Pang, Z.P., 2017. Enhanced AMPA receptor trafficking mediates the anorexigenic effect of endogenous glucagon-like peptide-1 in the paraventricular hypothalamus. Neuron 96, 897–909 e5.

Maniscalco, J.W., Rinaman, L., 2017. Interoceptive modulation of neuroendocrine, emotional, and hypophagic responses to stress. Physiol. Behav. 176, 195–206.

Maniscalco, J.W., Kreisler, A.D., Rinaman, L., 2013. Satiation and stress-induced hypophagia: examining the role of hindbrain neurons expressing prolactin-releasing Peptide or glucagon-like Peptide 1. Front. Neurosci. 6, 199.

Maniscalco, J.W., Zheng, H., Gordon, P.J., Rinaman, L., 2015. Negative energy balance blocks neural and behavioral responses to acute stress by "silencing" central glucagon-like peptide 1 signaling in rats. J. Neurosci. 35, 10701–10714.

McLean, I.W., Nakane, P.K., 1974. Periodate-lysine-paraformldehyde fixative. A new fixative for immunoelectron microscopy. J. Histochem. Cytochem. 22, 1077–1083.

Merchenthaler, I., Lane, M., Shughrue, P., 1998. Distribution of pre-pro-glucagon and glucagon-like peptide-1 receptor messenger RNAs in the rat central nervous system. J. Comp. Neurol. 403, 261–280.

Ong, Z.Y., Liu, J.-J., Pang, Z.P., Grill, H.J., 2017. Paraventricular thalamic control of food intake and reward: role of glucagon-like peptide-1 receptor signaling. Neuropsychopharmacology 42, 2387–2397.

Povysheva, N.V., Gonzalez-Burgos, G., Zaitsev, A.V., Kroner, S., Barrionuevo, G., Lewis, D.A., Krimer, L.S., 2006. Properties of excitatory synaptic responses in fast-spiking interneurons and pyramidal cells from monkey and rat prefrontal cortex. Cerebr. Cortex 16, 541–552.

Radley, J.J., Gosselink, K.L., Sawchenko, P.E., 2009. A discrete GABAergic relay mediates medial prefrontal cortical inhibition of the neuroendocrine stress response. J. Neurosci. 29, 7330–7340.

Rodríguez-Sierra, O.E., Turesson, H.K., Pare, D., 2013. Contrasting distribution of physiological cell types in different regions of the bed nucleus of the stria terminalis. J. Neurophysiol. 110, 2037–2049.

Sawchenko, P.E., Swanson, L.W., 1983. The organization and biochemical specificity of afferent projections to the paraventricular and supraoptic nuclei. In: Progress in Brain Research. Elsevier, pp. 19–29.

Shin, J.-W., Geerling, J.C., Loewy, A.D., 2008. Inputs to the ventrolateral bed nucleus of the stria terminalis. J. Comp. Neurol. 511, 628–657.

Simerly, R.B., Swanson, L.W., 1988. Projections of the medial preoptic nucleus: a Phaseolus vulgaris leucoagglutinin anterograde tract-tracing study in the rat. J. Comp. Neurol. 270, 209–242.

Smith, N.K., Hackett, T.A., Galli, A., Flynn, C.R., 2019. GLP-1: molecular mechanisms and outcomes of a complex signaling system. Neurochem. Int. 128, 94–105.

Sun, N., Cassell, M.D., 1993. Intrinsic GABAergic neurons in the rat central extended amygdala. J. Comp. Neurol. 330, 381–404.

Swanson, L.W., 2018. Brain maps 4.0—structure of the rat brain: an open access atlas with global nervous system nomenclature ontology and flatmaps. https://doi.org/10.1002/cne.24381.

Swanson, L.W., Sawchenko, P.E., 1980. Paraventricular nucleus: a site for the integration of neuroendocrine and autonomic mechanisms. Neuroendocrinology 31, 410–417.

Thompson, R., 2003. Structural characterization of a hypothalamic visceromotor pattern generator network. Brain Res. Rev. 41, 153–202.

Thorens, B., Porret, A., Buhler, L., Deng, S.-P., Morel, P., Widmann, C., 1993. Cloning and functional expression of the human islet GLP-1 receptor: demonstration that Exendin-4 is an agonist and Exendin-(9-39) an antagonist of the receptor. Diabetes 42, 1678–1682.

vanDijk, G., Thiele, T.E., 1999. Glucagon-like peptide-1 (7-36) amide: a central regulator of satiety and interoceptive stress. Neuropeptides 33, 406–414.

Wang, Y., Kim, J., Schmit, M.B., Cho, T.S., Fang, C., Cai, H., 2019. A bed nucleus of stria terminalis microcircuit regulating inflammation-associated modulation of feeding. Nat. Commun. 10, 2769.

Watson, R.E., Wiegand, S.T., Clough, R.W., Hoffman, G.E., 1986. Use of cryoprotectant to maintain long-term peptide immunoreactivity and tissue morphology. Peptides 7, 155–159.

Williams, D.L., Lilly, N.A., Edwards, I.J., Yao, P., Richards, J.E., Trapp, S., 2018. GLP-1 action in the mouse bed nucleus of the stria terminalis. Neuropharmacology 131, 83–95.

Zheng, H., Reiner, D.J., Hayes, M.R., Rinaman, L., 2019. Chronic suppression of glucagon-like peptide-1 receptor (GLP1R) mRNA translation in the rat bed nucleus of the stria terminalis reduces anxiety-like behavior and stress-induced hypophagia, but prolongs stress-induced elevation of plasma corticosterone. J. Neurosci. 39, 2649–2663.